ELSEVIER

Physica D 152–153 (2001) 145–162

PHYSICA D

www.elsevier.com/locate/physd

Some remarks on a WKB method for the nonselfadjoint Zakharov–Shabat eigenvalue problem with analytic potentials and fast phase

Peter D. Miller[1]

Department of Mathematics and Statistics, Monash University, Clayton, Vic. 3168, Australia

Dedicated to V.E. Zakharov on the occasion of his 60th birthday

Abstract

A formal method for approximating eigenvalues of the nonselfadjoint Zakharov–Shabat eigenvalue problem in the semi-classical scaling is described. Analyticity of the potential is assumed and appears to be crucial. The method involves finding appropriate paths between pairs of complex turning points, and reproduces the Y-shaped spectra observed by Bronski [Physica D 97 (1996) 376]. An application to all-optical ultrashort pulse generation is briefly described, and the kind of tools that are required to make the results rigorous are indicated. © 2001 Elsevier Science B.V. All rights reserved.

Keywords: WKB methods; Nonselfadjoint eigenvalue problems

1. Introduction

The nonselfadjoint Zakharov–Shabat eigenvalue problem is the first-order system of differential equations

$$\hbar \begin{bmatrix} u_1'(x;\lambda) \\ u_2'(x;\lambda) \end{bmatrix} = \begin{bmatrix} -\mathrm{i}\lambda & A(x)\exp\left(\dfrac{\mathrm{i}S(x)}{\hbar}\right) \\ -A(x)\exp\left(\dfrac{-\mathrm{i}S(x)}{\hbar}\right) & \mathrm{i}\lambda \end{bmatrix} \begin{bmatrix} u_1(x;\lambda) \\ u_2(x;\lambda) \end{bmatrix}, \tag{1}$$

where $\lambda \in \mathbb{C}$ is a complex eigenvalue parameter, and prime denotes differentiation with respect to x. The real-valued functions $A(x) > 0$ and $S(x)$ are given potentials, and $\hbar$ is a positive parameter. This linear eigenvalue problem was put forward by Zakharov and Shabat [11] as one half of the Lax pair for the solution of the focusing nonlinear Schrödinger equation by the inverse-scattering transform method. The corresponding nonlinear initial value problem for the complex field $\psi(x,t)$ is

$$\mathrm{i}\hbar\partial_t\psi + \frac{\hbar^2}{2}\partial_x^2\psi + |\psi|^2\psi = 0, \quad \psi(x,0) = A(x)\exp\left(\frac{\mathrm{i}S(x)}{\hbar}\right). \tag{2}$$

E-mail address: millerpd@math.lsa.umich.edu (P.D. Miller).

[1] Present address: Department of Mathematics, University of Michigan, East Hall, 525 E. University Avenue, Ann Arbor, MI 48109, USA.

PII: S0167-2789(01)00166-X

The first step in studying the behavior of solutions of this initial value problem in the semiclassical limit of $\hbar \downarrow 0$ is therefore the asymptotic spectral analysis of the scattering problem (1) as $\hbar \downarrow 0$ while the functions $A(x)$ and $S(x)$ are held fixed.

The eigenvalue problem (1) is not selfadjoint, or more precisely (1) cannot be written as the eigenvalue problem for any selfadjoint operator with some function of λ playing the role of the eigenvalue, and consequently the spectrum is not confined to any particular curve in the complex λ-plane for fixed $\hbar > 0$. The spectrum is symmetric under complex-conjugation, and the continuous spectrum includes the entire real λ-axis. Beyond these facts, there is the analytical "shadow bound" of Deift, Venakides and Zhou: [2] that all discrete eigenvalues lie in the "$\mathcal{O}(\hbar)$-blurred" shadow of the curve $\lambda = \lambda(x)$ given parametrically by

$$(\lambda + \tfrac{1}{2}S'(x))^2 + A(x)^2 = 0, \quad x \in \mathbb{R} \tag{3}$$

plus a strip of uniform width $\mathcal{O}(\hbar)$ around the real axis. This estimate excludes neither the possibility of eigenvalues accumulating in open domains of the complex λ-plane, nor that of eigenvalues accumulating near, but not on, the real axis as $\hbar$ tends to zero.

Very careful numerical calculations carried out by Bronski [2] seemed to indicate that there was, however, more to the story. These experiments strongly suggested that at least for some fixed real functions $A(x)$ and $S(x)$, the discrete eigenvalues of (1) accumulate in the limit $\hbar \downarrow 0$ on some system of curves in the complex λ-plane, that the total number of eigenvalues scales like $\hbar^{-1}$, and that the discrete spectral measures converge to something that has singular support on the curves, but that is absolutely continuous with respect to Lebesgue measure when restricted to the curves.

It is pointed out in that same paper that these features are not captured by a direct WKB analysis of the differential equation (1) because unless λ satisfies (3) for some real x, there are no real turning points and the WKB eigenfunctions do not appear to break down for any real x. The "paradox" of this kind of WKB analysis is that every value of λ that is contained within the turning point curve defined by (3) appears to be an eigenvalue, whereas every other value of λ appears not to be an eigenvalue. These formal results are in contradiction with the numerical experiments, which show that eigenvalues can accumulate on curves either inside or outside the turning point curve.

In this paper, we show how an appropriate complexification of the WKB method allows the calculation of the curves of spectral accumulation, and also the asymptotic density of eigenvalues on the curves. The method we describe is formal, and rigorous proofs that the WKB eigenvalues provided by the method are accurate up to errors that are $o(\hbar)$ will be given in a future publication. We describe the procedure in general in Section 2, and then in Section 3 we apply it to the specific case $A(x) = S(x) = \operatorname{sech}(2x)$, for which Bronski's experiments indicated the asymptotic appearance of a fascinating "Y-shaped" semiclassical spectrum. The spectral curves predicted by our method agree with the published numerical results. We briefly describe in Section 4 an application of the method to the problem of ultrashort pulse generation in optical fibers, and finally offer in Section 5 some indications of how some of these formal results might be proved.

2. Description of the method

2.1. Reduction to the Schrödinger equation with a complex potential

It is straightforward to rewrite the system of first-order equations (1) as a semiclassically scaled Schrödinger equation with a slightly perturbed complex-valued potential. To do this, suppose that λ is not on the turning point

[2] This is referenced in [2] as a private communication, but to date seems not to have appeared elsewhere in the literature.

curve defined by (3) and make the change of variables

$$y_{\pm}(x;\lambda) = \frac{u_2(x;\lambda)\exp(\mathrm{i}S(x)/(2\hbar)) \pm u_1(x;\lambda)\exp(-\mathrm{i}S(x)/(2\hbar))}{\sqrt{A(x) \pm \mathrm{i}(\lambda + S'(x)/2)}}, \tag{4}$$

where an arbitrary smooth nonvanishing branch of the square root is selected in each case. One then finds that (1) is equivalent to the two independent eigenvalue equations

$$\hbar^2 y_{\pm}''(x;\lambda) = \{V_0(x;\lambda) + \hbar^2 F_{\pm}(x;\lambda)\}y_{\pm}(x;\lambda), \tag{5}$$

where the leading-order potential $V_0(x;\lambda)$ is given by

$$V_0(x;\lambda) = -[(\lambda + \tfrac{1}{2}S'(x))^2 + A(x)^2], \tag{6}$$

and the corrections are given by

$$F_{\pm}(x;\lambda) = \frac{1}{2}\left[\left[\log\left(A(x) \pm \mathrm{i}\left(\lambda + \frac{S'(x)}{2}\right)\right)\right]'\right]^2 - \frac{[(A(x) \pm \mathrm{i}(\lambda + S'(x)/2))^{1/2}]''}{(A(x) \pm \mathrm{i}(\lambda + S'(x)/2))^{1/2}}. \tag{7}$$

Let us restrict attention to those potentials for which $A(x)$ and $S'(x)$ vanish sufficiently rapidly as $|x| \to \infty$. Then, it is easy to see that the change of variables does not alter the notion of discrete spectrum; that is, finding the discrete spectrum of (1) is equivalent to finding the values of λ with $\Im(\lambda) > 0$ for which (5) has an $L^2(\mathbb{R})$ solution. Note that by construction, the two Schrödinger equations rpresented by Eq. (5) for $y_+(x;\lambda)$ and $y_-(x;\lambda)$ have the *same* discrete spectrum, since they both come from the same eigenvalue problem (1). The ratio $y_+(x;\lambda)/y_-(x;\lambda)$ of bound states at an eigenvalue λ, although bounded in x, may not have the same limiting value as x tends to positive and negative infinity. Also, with this restriction the corrections $F_{\pm}(x;\lambda)$ to the potential are uniformly bounded rapidly decreasing functions of real x.

Our goal is to compute each eigenvalue λ of (5) up to an error of size $\mathrm{o}(\hbar)$, since with this accuracy and the assumption that the eigenvalues are separated by a quantity whose reciprocal is $\mathcal{O}(\hbar^{-1})$, we can obtain a leading-order formula for the asymptotic spectral measure. A claim that we leave unjustified at the moment is that for this purpose it is sufficient to determine the discrete spectrum of the equation

$$\hbar^2 y''(x;\lambda) = V_0(x;\lambda)y(x;\lambda) \tag{8}$$

with the same accuracy. That is, each eigenvalue of (5) is $\mathcal{O}(\hbar^2)$ away from an eigenvalue of (8). This statement requires a perturbation argument that we outline in Section 5. In any case, from now on we focus attention on the asymptotic spectral analysis of the reduced problem (8).

2.2. *Finding real paths between pairs of complex turning points. Complex arcs of asymptotic spectrum*

Consider for a moment the selfadjoint case of (8) when the function $V_0(x;\lambda)$ is a real-valued function of x for some λ; more precisely, a potential well. One of the important heuristics used in constructing solutions $y(x;\lambda)$ of (8) in this case is that the leading-order WKB solutions $V_0(x;\lambda)^{-1/4}\exp(\phi(x;\lambda)/\hbar)$ with $(\phi'(x;\lambda))^2 = V_0(x;\lambda)$ are only to be trusted in as much as they are not exponentially large as $\hbar \downarrow 0$. Thus, one assumes exponentially small decaying solutions outside the turning points, and matches through the two turning points on each side into a central region where the WKB eigenfunctions, though not exponentially small, are bounded. It is here that the matching takes place determining the WKB eigenvalues $\lambda = \lambda_k^{\mathrm{WKB}}$. Matching from the oscillatory region out into the classically forbidden region is not sensible because exponentially small matching errors can lead to unbounded

errors in the forbidden region. The heuristic of working with only bounded solutions therefore appears in this context in the form of the "directional character of connection formulae" [4].

Since in our application the potential function $V_0(x;\lambda)$ is complex-valued for $\Im(\lambda) > 0$, we have no real turning points for all λ except for those satisfying (3). If we assume the potential functions $A(x)$ and $S(x)$ to be real-analytic, then we may consider studying the asymptotics of solutions of (8) on some contour in the complex x-plane connecting $-\infty$ to $+\infty$ and lying "near" the real axis, in hopes of threading the contour through a pair of complex turning points and applying similar matching heuristics as in the selfadjoint case. Given a pair of complex roots $x_+(\lambda)$ and $x_+(\lambda)$ of $V_0(x;\lambda) = 0$, an analogous treatment becomes possible if there exists an "appropriate" contour C connecting $x = -\infty$ to $x = +\infty$ via the two complex turning points $x_-(\lambda)$ and $x_+(\lambda)$. We write $C = (C_-, C_0, C_+)$ where C_- connects $x = -\infty$ to $x = x_-(\lambda)$, C_0 connects $x = x_-(\lambda)$ to $x = x_+(\lambda)$, and C_+ connects $x = x_+(\lambda)$ to $x = +\infty$. Let λ be fixed. By "appropriate", we mean that the following four conditions hold:

1. The function $V_0(x;\lambda)$ is holomorphic in x for all x in the region of the complex x-plane enclosed by C and the real x-axis.
2. For all $x \in C_-$,
$$\Re\left\{\int_{x_-(\lambda)}^{x} \sqrt{V_0(z;\lambda)}\,\mathrm{d}z\right\} \neq 0 \tag{9}$$
with the integral being taken along C_-, and C_- can be chosen so that the angle between C_- and C_0, measured in either the positive or negative direction, is greater than $2\pi/3$.
3. For all $x \in C_+$,
$$\Re\left\{\int_{x_+(\lambda)}^{x} \sqrt{V_0(z;\lambda)}\,\mathrm{d}z\right\} \neq 0 \tag{10}$$
with the integral being taken along C_+, and C_+ can be chosen so that the angle between C_+ and C_0, measured in either the positive or negative direction, is greater than $2\pi/3$.
4. For all $x \in C_0$,
$$\Re\left\{\int_{x_-(\lambda)}^{x} \sqrt{V_0(z;\lambda)}\,\mathrm{d}z\right\} = 0 \tag{11}$$
with the integral being taken along C_0. We call C_0 a *real path*.

The first item is needed to ensure that the approximate eigenfunction can be continued back to the real x-axis (see Section 5). The next two items ensure the existence of an exponentially small WKB eigenfunction outside the turning points (the angle condition is a technical one required for good behavior of the local WKB eigenfunction near the turning points). Because these two criteria are inequalities, there is some freedom in the precise placement of the "decay" paths C_- and C_+; for later simplicity, we assume that for sufficiently large $|x|$, C_- and C_+ lie on the real axis. The fourth item ensures that the turning points are connected by a path on which *both* WKB eigenfunctions are bounded as $\hbar$ tends to zero.

This final item is the most illuminating, as it is easily reinterpreted as a differential equation for the real path C_0 in the complex x-plane. If $x = u + \mathrm{i}v$, then a field of curves is defined by the differential relation

$$\Re\{\sqrt{V_0(u+\mathrm{i}v;\lambda)}(\mathrm{d}u + \mathrm{i}\,\mathrm{d}v)\} = 0. \tag{12}$$

An appropriate real path C_0 exists when this differential equation has a heteroclinic orbit connecting the two fixed

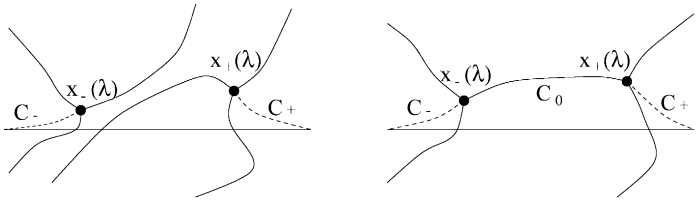

Fig. 1. The complex x-plane. Left: for λ not on an asymptotic spectral arc, there is no real path connecting $x_-(\lambda)$ and $x_+(\lambda)$. Right: for λ on an asymptotic spectral arc, the real path C_0 exists connecting the two complex turning points. Note that by the square root vanishing of $\sqrt{V_0(x;\lambda)}$ at the turning points, there are three candidate real paths emanating from each turning point.

points $x_-(\lambda)$ and $x_+(\lambda)$. Suppose that for a pair of complex turning points we have the condition

$$\Re\left\{\int_{x_-(\lambda)}^{x_+(\lambda)}\sqrt{V_0(z;\lambda)}\,\mathrm{d}z\right\}=0. \tag{13}$$

Then, there exists an orbit of (12) that connects the two endpoints. This orbit is a candidate for a real path if in addition it does not pass through the point at $x=\infty$, or through any other points of nonanalyticity of $\sqrt{V_0(x;\lambda)}$.

We can perhaps emphasize at this point that, given a pair of turning points that are distinct throughout a domain in the complex λ-plane, the reality relation (13) itself determines a curve in the complex λ-plane. If λ is on one of these curves, then subject to the heteroclinic orbit C_0 avoiding any singularities and the existence of appropriate "decay" paths C_+ and C_-, the standard WKB procedure can be expected to apply to determine whether λ is in fact an $\mathrm{o}(\hbar)$ distance away from an eigenvalue. We therefore expect that as $\hbar$ tends to zero, the discrete eigenvalues of (8) will accumulate on the union of curves in the complex λ-plane described by the formula (13), with the union being taken over pairs of complex turning points. The curves in the complex λ-plane on which all four conditions are satisfied, giving rise to an admissible contour $C=(C_-,C_0,C_+)$, will be called *asymptotic spectral arcs*. See Fig. 1.

In Section 5, we outline how perturbation methods can be used to show that existence of a WKB eigenfunction of the reduced Schrödinger equation, Eq. (8) implies that of a *true* eigenfunction of (8), for a suitable adjustment (by $\mathcal{O}(\hbar^2)$) of the WKB eigenvalue. This argument holds *on the special contour* $C=(C_-,C_0,C_+)$. An additional step is then required in the rigorous analysis to show that no errors are introduced in the analytic continuation of the true eigenfunction back down to the real axis. Once we have an eigenfunction of (8) *on the real axis*, we then invoke perturbation theory once again to show the existence of an eigenfunction of (5), and therefore of the original Zakharov–Shabat eigenvalue problem (1), with a nearby eigenvalue.

2.3. Bohr–Sommerfeld quantization on the arcs. Asymptotic distribution of proportionality constants

Applying standard WKB theory [4] on the contour $C=(C_-,C_0,C_+)$, either through matching expansions or by constructing uniformly valid approximations with the help of the parabolic cylinder equation, one finds the eigenvalue condition

$$\frac{1}{\pi\hbar}\Im\left\{\int_{x_-(\lambda)}^{x_+(\lambda)}\sqrt{V_0(z;\lambda)}\,\mathrm{d}z\right\}-\frac{1}{2}\in\mathbb{Z}, \tag{14}$$

which can be interpreted as a Bohr–Sommerfeld quantization rule for λ on the appropriate asymptotic spectral arc corresponding to the condition (13) with the turning points $x_-(\lambda)$ and $x_+(\lambda)$. Given a real parameterization $\lambda=\lambda(s)$

of the arc, the asymptotic spectral measure on the arc is

$$\mathrm{d}\mu^{\mathrm{WKB}}(s) = \frac{1}{\pi\hbar}\frac{\mathrm{d}}{\mathrm{d}s}\left|\Im\left\{\int_{x_-(\lambda(s))}^{x_+(\lambda(s))}\sqrt{V_0(z;\lambda(s))}\,\mathrm{d}z\right\}\right|\mathrm{d}s. \tag{15}$$

In the asymptotic analysis of the inverse-scattering problem [7], it appears to be important to know that the error in this leading-order formula (15) for the asymptotic discrete spectral measure is not merely $\mathcal{O}(1)$ (the measure itself is $\mathcal{O}(1/\hbar)$), but actually an order of magnitude smaller, $\mathcal{O}(\hbar)$. Estimation of the error requires analysis significantly more detailed than that outlined in Section 5, which is concerned only with one eigenvalue at a time, and then with only crude convergence properties.

Associated with each discrete eigenvalue λ_k of the Zakharov–Shabat eigenvalue problem (1) with $\Im(\lambda_k) > 0$, and equally important in the inverse-scattering theory, is a *proportionality constant* γ_k defined as follows. Let the eigenfunction be normalized as $x \to -\infty$ by the condition

$$\lim_{x\to-\infty}\begin{bmatrix} u_1(x;\lambda_k)\\ u_2(x;\lambda_k)\end{bmatrix}\exp\left(\frac{\mathrm{i}\lambda_k x}{\hbar}\right) = \begin{bmatrix}1\\0\end{bmatrix}. \tag{16}$$

Then, the proportionality constant is determined by the asymptotics for $x \to +\infty$:

$$\lim_{x\to+\infty}\begin{bmatrix} u_1(x;\lambda_k)\\ u_2(x;\lambda_k)\end{bmatrix}\exp\left(\frac{-\mathrm{i}\lambda_k x}{\hbar}\right) = \frac{1}{\gamma_k}\begin{bmatrix}0\\1\end{bmatrix}. \tag{17}$$

Let $n_\pm(\lambda)$ denote the increment of the argument of $A(x) \pm \mathrm{i}(\lambda + \frac{1}{2}S'(x))$ as x varies from $-\infty$ to $+\infty$, divided by 2π. Denote by $\bar{S}_\infty$ the mean asymptotic phase:

$$\bar{S}_\infty = \tfrac{1}{2}(S(-\infty) + S(+\infty)). \tag{18}$$

Then, by the change of variables $(u_1, u_2) \mapsto (y_+, y_-)$, the proportionality constant can be defined in two ways:

$$\gamma_k = (-1)^{n_+(\lambda_k)}\exp\left(\frac{-\mathrm{i}\bar{S}_\infty}{\hbar}\right)\lim_{x\to+\infty}\frac{y_+(-x;\lambda_k)}{y_+(x;\lambda_k)} = -(-1)^{n_-(\lambda_k)}\exp\left(\frac{-\mathrm{i}\bar{S}_\infty}{\hbar}\right)\lim_{x\to+\infty}\frac{y_-(-x;\lambda_k)}{y_-(x;\lambda_k)}. \tag{19}$$

When the eigenvalue λ_k is "inside" the turning point curve defined by (3), then the index $n_+(\lambda_k) + n_-(\lambda_k)$ of the quantity $A(x)^2 + (\lambda + \frac{1}{2}S'(x))^2$ is odd [2]. In this case, it is easy to see that

$$\lim_{x\to+\infty}\frac{y_+(-x;\lambda_k)}{y_+(x;\lambda_k)} = \lim_{x\to+\infty}\frac{y_-(-x;\lambda_k)}{y_-(x;\lambda_k)}. \tag{20}$$

For eigenvalues inside the turning point curve, it therefore appears to be possible to deduce a leading-order formula for the proportionality constants γ_k from the appropriately constructed global WKB solutions of (8) for $y(x;\lambda_k^{\mathrm{WKB}})$. That is, one can obtain a consistent asymptotic formula for γ_k by substituting a uniformly valid approximation $y^{\mathrm{WKB}}(x;\lambda_k^{\mathrm{WKB}})$ for *either* $y_+(x;\lambda_k)$ or $y_-(x;\lambda_k)$ in (19). For eigenvalues outside the turning point curve, the large $|x|$ asymptotics of at least one of the functions $y_+(x;\lambda_k)$ or $y_-(x;\lambda_k)$ will not agree with those of the bound state $y(x;\lambda_0)$ and therefore it is not clear how to determine the proportionality constants from properties of the solutions of the reduced equation, Eq. (8).

Moreover, note that while an eigenvalue λ of (5) and an eigenvalue λ_0 of (8) may be $\mathrm{o}(\hbar)$ close, the corresponding $L^2(\mathbb{R})$ eigenfunctions, when normalized so that

$$\frac{y_\pm(x;\lambda)}{y(x;\lambda_0)}\exp\left(\frac{\mathrm{i}(\lambda-\lambda_0)x}{\hbar}\right) \to 1, \qquad x \to -\infty, \tag{21}$$

may not satisfy

$$\frac{y_\pm(x;\lambda)}{y(x;\lambda_0)}\exp\left(\frac{-\mathrm{i}(\lambda-\lambda_0)x}{\hbar}\right)\to 1+\mathrm{o}(1),\qquad x\to+\infty. \tag{22}$$

That is, true eigenfunctions and approximate eigenfunctions may not define the same proportionality constants. Clearly, more work is required to obtain accurate information about the distribution of the γ_k as $\hbar$ tends to zero. An accurate formula for the distribution of the γ_k appears to be a key ingredient in the finite time analysis of the inverse-scattering problem in the semiclassical limit [7].

3. Application: the Y-shaped spectra observed by Bronski

Here, we apply the method to a special case studied by Bronski [2]. Namely, we take

$$A(x)=S(x)=\operatorname{sech}(2x). \tag{23}$$

The first step is to catalog for fixed $\lambda\in\mathbb{C}$ the zeros in the complex x-plane of $-V_0(x;\lambda)=(\lambda+\frac{1}{2}S'(x))^2+A(x)^2$. These are the complex turning points. In this case, the potential $V_0(x;\lambda)$ is periodic with fundamental period $\pi\mathrm{i}$. In the *fundamental period strip* $-\pi/2<\Im(x)\le\pi/2$ of the complex x-plane, there are two fourth-order poles of $V_0(x;\lambda)$ located at $x=\pm\mathrm{i}\pi/4$ (for all λ). There are also eight λ-dependent zeros of $V_0(x;\lambda)$ in each period strip, typically distinct and therefore simple. When λ is purely imaginary, there are four zeros in each strip that lie on the imaginary x-axis, two between each pair of poles; the remaining four zeros in the fundamental period strip make up a quartet: $(x,-x,x^*,-x^*)$. For λ not purely imaginary, this nice symmetry of the complex turning points is broken.

For some λ, there can be double zeros of $V_0(x;\lambda)$. These are not difficult to characterize, simply by considering simultaneously the equations $V_0(x;\lambda)=0$ and $V_0'(x;\lambda)=0$. It is interesting to consider embedding the potential in a family indexed by a parameter ξ:

$$-V_{0,\xi}(x;\lambda)=(\lambda+\tfrac{1}{2}\xi S'(x))^2+A(x)^2, \tag{24}$$

so that $V_0(x;\lambda)=V_{0,1}(x;\lambda)$. Then, the double roots appear for only four values of $\lambda=\lambda_\mathrm{D}$:

$$\lambda_\mathrm{D}=\mathrm{i}\sigma\sqrt{\frac{1}{2}+\frac{1+\tau\sqrt{1-8\xi^2}}{8\xi^2}}\left(1-\frac{1+\tau\sqrt{1-8\xi^2}}{4}\right),\quad \sigma=\pm1,\ \ \tau=\pm1. \tag{25}$$

and are given by the solution of the transcendental equation

$$\tanh(2x)=\frac{1+\tau\sqrt{1-8\xi^2}}{4\mathrm{i}\sigma\xi}. \tag{26}$$

For $0<\xi<1/\sqrt{8}$, the values $\lambda=\lambda_\mathrm{D}$ for which there exist double roots of $V_{0,\xi}(x;\lambda)=0$ lie on the imaginary axis, while for $\xi>1/\sqrt{8}$ these values of λ form a quartet: $(\lambda,-\lambda,\lambda^*,-\lambda^*)$. The value $\xi=1/\sqrt{8}$ was obtained in [2] with the use of a "fixed but small $\hbar$" perturbation argument to determine the value of ξ for which the eigenvalues first move off of the imaginary axis into the complex plane, ultimately (for $\xi=1$) forming the branches of a "Y-shaped" spectrum. We will soon see that taking $\xi=1$ in the above formula for the special values of λ yields the endpoints of the two branches of the Y in the complex λ-plane. The particular numerical values we obtain are

$$\lambda_\mathrm{D}=\mathrm{i}\sigma\sqrt{\frac{1}{2}+\frac{1+\mathrm{i}\tau\sqrt{7}}{8}}\left(1-\frac{1+\mathrm{i}\tau\sqrt{7}}{4}\right),\quad \sigma=\pm1,\ \ \tau=\pm1, \tag{27}$$

which give excellent predictions of the endpoints of the branches of the Y as seen in Bronski's numerical experiments [2].

We first determine eight distinct complex turning points in the fundamental period strip for $\lambda = 0.2\mathrm{i}$ in order to later apply analytic continuation to the roots with respect to λ. The deformation $0 < \xi \leq 1$ is useful in obtaining the turning points for the potentials (23). When $\xi = 0$, there are four roots labeled as follows: x_1 is the negative real root, and $x_3 = x_1 + \mathrm{i}\pi/2$. x_2 is the positive real root, and $x_4 = x_2 + \mathrm{i}\pi/2$. Applying analytic continuation to these distinct roots with respect to the parameter ξ allows these four roots to be calculated for $\xi = 1$. The pair x_1 and x_2 moves into the lower half-plane, maintaining the symmetry $x_2 = -x_1^*$. The pair x_3 and x_4 undergoes a similar process along the way to $\xi = 1$. The four remaining roots in the fundamental period strip for $\xi = 1$ are on the imaginary axis and are labeled x_5, x_6, x_7, and x_8 in order of increasing imaginary part. So, x_5 lies below $-\mathrm{i}\pi/4$, x_6 lies between $-\mathrm{i}\pi/4$ and zero, x_7 lies between zero and $\mathrm{i}\pi/4$, and x_8 lies above $\mathrm{i}\pi/4$. This process gives us an unambiguous labeling of the eight roots in the fundamental period strip for $\xi = 1$ and $\lambda = 0.2\mathrm{i}$. Fixing now $\xi = 1$, we obtain the roots for other values of λ by analytically continuing these along the "L-shaped" path from $0.2i$ to $\Re(\lambda) + 0.2\mathrm{i}$ and then from $\Re(\lambda) + 0.2\mathrm{i}$ to λ.

We have already calculated the four values of $\lambda = \lambda_\mathrm{D}$ for which there are double roots in the complex x-plane. These are branch points for the root functions $x_\mathrm{i}(\lambda)$ defined above, and using the branches defined above by our L-shaped path of continuation, the branch cuts emanate from the branch points and are straight vertical rays connecting each branch point to infinity. The monodromy around each branch point is as follows. For a counterclockwise analytic continuation of the roots around the endpoint λ_D in the first quadrant:

$$\begin{aligned} &x_1 \to x_1, \qquad x_2 \to x_6, \qquad x_3 \to x_5 + \pi\mathrm{i}, \qquad x_4 \to x_4, \\ &x_5 \to x_3 - \pi\mathrm{i}, \qquad x_6 \to x_2, \qquad x_7 \to x_7, \qquad x_8 \to x_8. \end{aligned} \tag{28}$$

Similarly, for a counterclockwise analytic continuation of the roots around the endpoint λ_D in the second quadrant:

$$\begin{aligned} &x_1 \to x_6, \qquad x_2 \to x_2, \qquad x_3 \to x_3, \qquad x_4 \to x_5 + \pi\mathrm{i}, \\ &x_5 \to x_4 - \pi\mathrm{i}, \qquad x_6 \to x_1, \qquad x_7 \to x_7, \qquad x_8 \to x_8. \end{aligned} \tag{29}$$

The next step is to determine the values of λ for which there exists a contour consisting of a real path C_0 between two complex turning points along with two decay paths C_- and C_+. These are the values of λ for which WKB analysis becomes possible for determining the eigenvalues. For each pair of complex turning points, we can consider the complex-valued integral appearing in the relation (13). Denote this integral by

$$I_{jk}(\lambda) = \int_{x_j(\lambda)}^{x_k(\lambda)} \sqrt{V_0(z;\lambda)}\,\mathrm{d}z. \tag{30}$$

In particular, we will want to consider $I_{12}(\lambda)$, $I_{16}(\lambda)$, and $I_{26}(\lambda)$. We construct well-defined branches of these functions by choosing straight-line paths of integration and definite signs of the square root for $\lambda = 0.2\mathrm{i}$ and applying analytic continuation along the same L-shaped path as was used to define the roots. The monodromy of the roots then implies that these three functions, along with their negatives, form six branches of the same analytic function defined on a six-sheeted Riemann surface over the λ-plane. See Fig. 2.

The conditions $\Re(I_{12}(\lambda)) = 0$, $\Re(I_{16}(\lambda)) = 0$, and $\Re(I_{26}(\lambda)) = 0$ yield three curves in the λ-plane. The images of these curves in the upper half-plane are plotted in Fig. 3 along with the turning point curve defined by (3) and the two branch points $\lambda = \lambda_\mathrm{D}$, indicated with circles. The curve $\Re(I_{12}(\lambda)) = 0$ coincides with the imaginary axis, the curve $\Re(I_{16}(\lambda)) = 0$ has negative slope, and the curve $\Re(I_{26}(\lambda)) = 0$ has positive slope. The other equations $\Re(I_{jk}(\lambda)) = 0$, as well as equations corresponding to pairs of turning points in different period strips, may also have solutions yielding curves in the λ-plane, but these curves play no role in the WKB analysis of the potentials

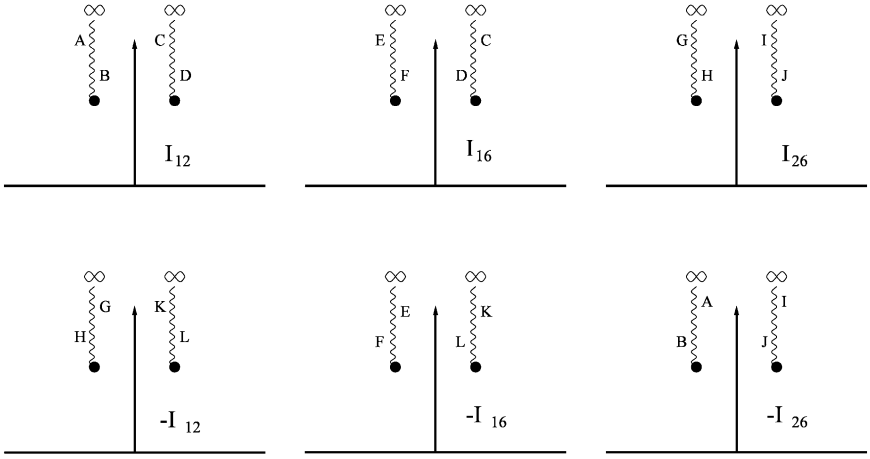

Fig. 2. The six branches of the complex phase integral over the upper half λ-plane. The branch points and the corresponding cuts are shown in each figure, and the letters near the cuts indicate how the six sheets are identified pairwise along the cuts.

(23) for the same kind of reasons that will shortly eliminate portions of the curves indicated in Fig. 3 from further consideration. For simplicity, we therefore restrict attention from now on to the three curves indicated in Fig. 3. The semiclassical spectra observed by Bronski [2] would seem to lie on the union of these three curves.

To continue the analysis of the points on the curves in Fig. 3, we must look more carefully at the complex x-plane, and the geometry of the solutions of the differential equation (12) therein. As a means of illustration, we used a simple Euler scheme to compute numerical approximations to the three orbits of (12) emerging at 120° angles from each fixed point $x_i(\lambda)$. We call these the *critical orbits* of (12). The first value of λ we consider is on the imaginary axis, which is the solution set of $\Re(I_{12}(\lambda)) = 0$, below the point of mutual intersection of all three curves. This situation is shown in Fig. 4. On the left is the λ-plane as in Fig. 3, with the value of λ under consideration indicated with a square box. On the right is a plot of the critical orbits of (12) in the fundamental period strip in the complex x-plane. The complex turning points are indicated with circles, and the fourth-order poles of the function $V(x;\lambda)$

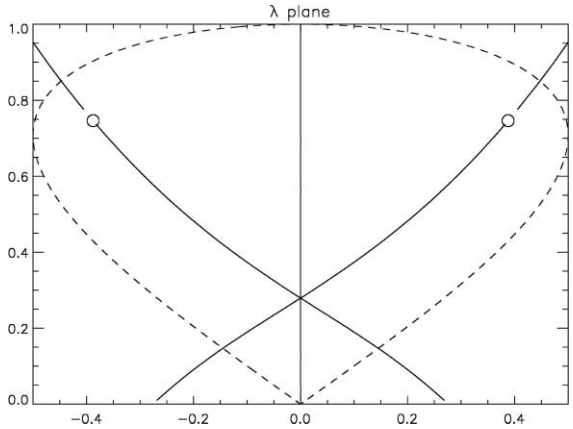

Fig. 3. The three curves $\Re(I_{12}(\lambda)) = 0$, $\Re(I_{16}(\lambda)) = 0$, and $\Re(I_{26}(\lambda)) = 0$. The dashed line is the turning point curve given by (3). The branch points where there exist double complex turning points are indicated with circles.

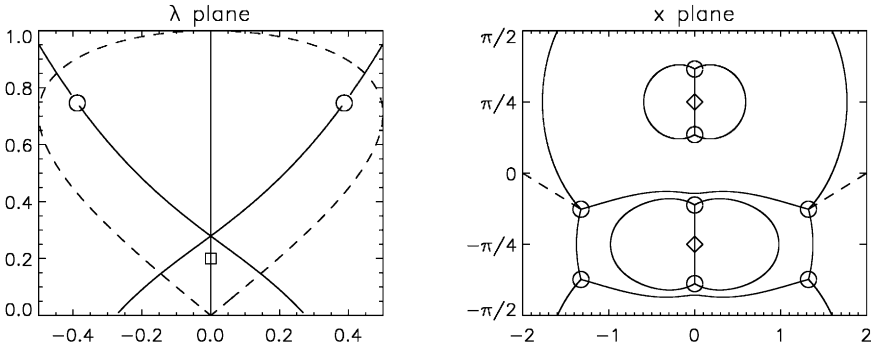

Fig. 4. The x-plane corresponding to $\lambda = 0.2\mathrm{i}$.

are indicated with diamonds. There is a real path C_0 connecting the complex turning points $x_1(\lambda)$ and $x_2(\lambda)$, and there also exist appropriate decay paths C_- and C_+, indicated schematically with dashed lines. As mentioned above, these decay paths are unlike the real path C_0 in that they are only determined by *inequalities* along with some global topological information, and therefore there is some freedom in their precise placement. However, in each case that we claim the decay contours C_+ and C_- exist, we have checked the relevant inequality numerically along the particular paths shown in the figure. Note that, while there are three orbits of (12) connected to each complex turning point, there are an infinite number of orbits meeting at each fourth-order pole. The local orbit structure of (12) near such a pole is illustrated in Fig. 5.

The critical orbits of (12) corresponding to a value of λ on the imaginary axis just below the triple intersection point of the curves in Fig. 3 is shown in Fig. 6. Here, we see that the complex turning point $x_6(\lambda)$ is moving up very close to the real path C_0 that continues to connect $x_1(\lambda)$ and $x_2(\lambda)$. The decay paths C_+ and C_- continue to exist as well. This proximity becomes more pronounced as λ approaches the triple intersection point, which occurs roughly for $\lambda = 0.28\mathrm{i}$. Fig. 7 shows the critical orbits of (12) in the complex x-plane at the triple intersection point. Clearly, the real path between $x_1(\lambda)$ and $x_2(\lambda)$ now passes *through* the third turning point $x_6(\lambda)$, meeting it in a corner with a 120° angle. This explains how the three conditions $\Re(I_{12}(\lambda)) = 0$, $\Re(I_{16}(\lambda)) = 0$, and $\Re(I_{26}(\lambda)) = 0$ are satisfied simultaneously at the triple intersection point. For this special value of λ, there is a connected chain of two heteroclinic orbits of (12). The decay paths C_+ and C_- exist and may be chosen as shown in the figure with dashed lines.

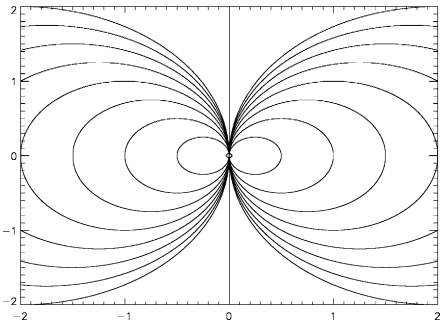

Fig. 5. The local orbit structure of (12) near a double pole of $\sqrt{V_0(x;\lambda)}$.

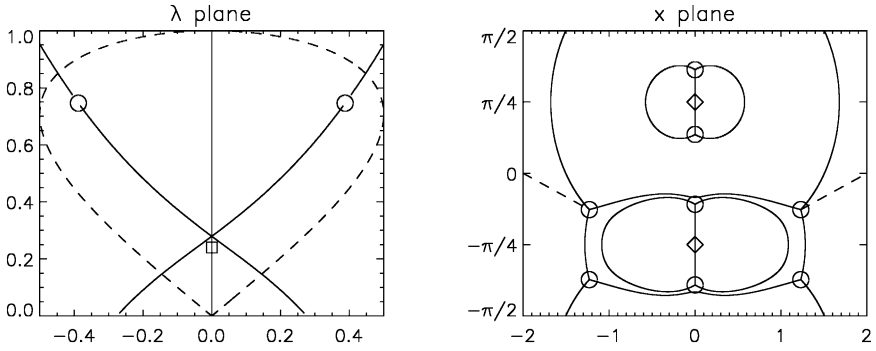

Fig. 6. The x-plane corresponding to $\lambda = 0.24\mathrm{i}$.

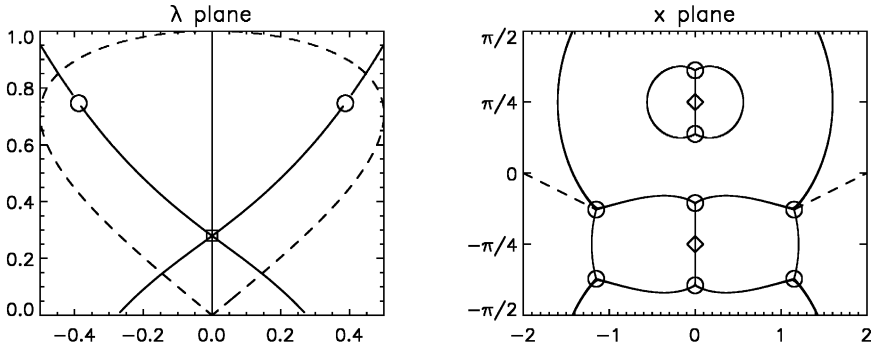

Fig. 7. The x-plane corresponding to $\lambda = 0.28\mathrm{i}$, essentially the triple intersection point of the three curves in Fig. 3.

We now consider how the degenerate situation at the triple intersection point unfolds along the remaining five directions in the complex λ-plane. First, we continue along the imaginary axis, the solution of $\Re(I_{12}(\lambda)) = 0$, just above the triple intersection point. The critical orbits of (12) are shown in Fig. 8 for this case. The essential observation is that the two halves of the real path C_0 now meet at a double pole of $\sqrt{V_0(x;\lambda)}$. This means that the WKB approximations have an essential singularity along the contour (C_-, C_0, C_+), and makes further WKB

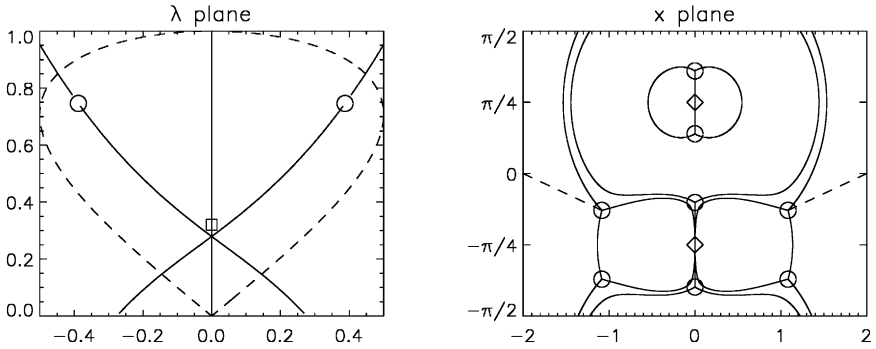

Fig. 8. The x-plane corresponding to $\lambda = 0.32\mathrm{i}$.

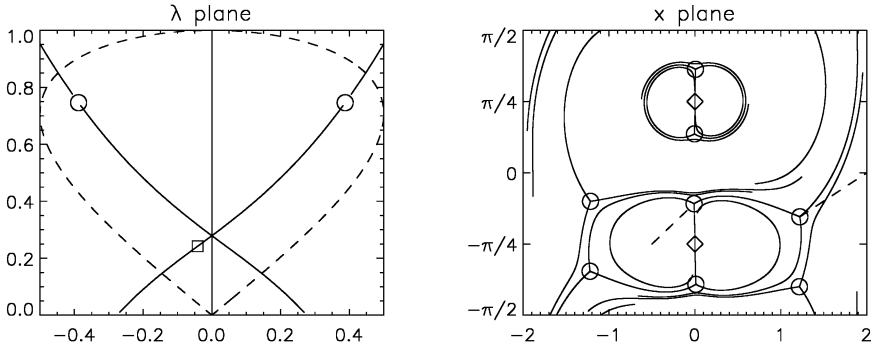

Fig. 9. The x-plane corresponding to a value of λ for which there exists a real path C_0 but no appropriate decay path C_-.

analysis impossible, even though appropriate decay paths C_+ and C_- exist. The same phenomenon continues for all λ on the imaginary axis above the triple intersection point. This restricts the WKB analysis to the portion of the curve $\Re(I_{12}(\lambda)) = 0$ that lies below the triple intersection point.

We now turn our attention to the graph of the relation $\Re(I_{26}(\lambda)) = 0$, which is the curve with positive slope in Fig. 3. We first consider a value of λ on this curve just below the triple intersection point. The critical orbits of (12) are shown in Fig. 9. We see that by unfolding the triple intersection point in this direction we maintain the half of the real path C_0 between $x_2(\lambda)$ and $x_6(\lambda)$ avoiding any singularities. The decay path C_+ is also preserved. However, it is not possible to find a decay path C_- connecting the turning point $x = x_6(\lambda)$ to $x = -\infty$. This is because the remaining two orbits of (12) emanating from $x = x_6(\lambda)$ close onto themselves and meet at the pole $x = -\mathrm{i}\pi/4$. Since all decay paths C_- must emerge from the turning point and stay between these two curves, it is impossible for any such curve to connect to $x = -\infty$. This phenomenon continues as λ moves away from the triple intersection point in this direction. WKB analysis is not possible along the portion of the graph of $\Re(I_{26}(\lambda)) = 0$ that lies below the triple intersection point.

The situation is more favorable when the triple intersection point is unfolded along the graph of $\Re(I_{26}(\lambda)) = 0$ in the other direction. As shown in Fig. 10, the passage through the triple intersection point causes one of the orbits emerging from $x_6(\lambda)$ to cross the separatrix, and this makes the point $x = -\infty$ reachable from the turning point by a decay path C_-. On this portion of the curve, WKB analysis is possible on the contour (C_-, C_0, C_+) in the complex x-plane. The possibility of WKB analysis continues as one moves up the graph of $\Re(I_{26}(\lambda)) = 0$ in the

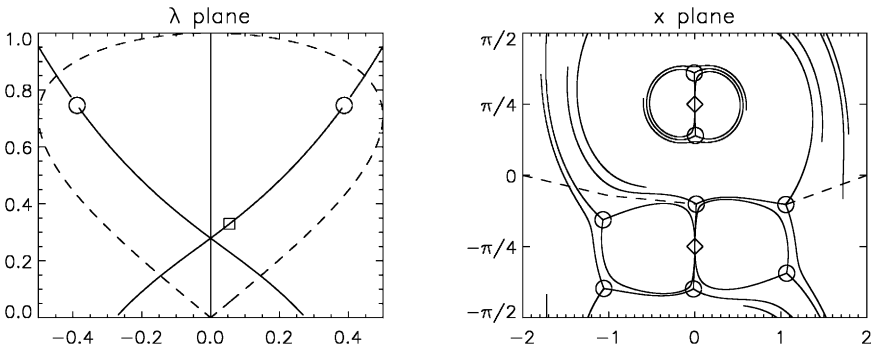

Fig. 10. The x-plane corresponding to a value of λ on a branch of the Y. Here there exists a real path C_0 and also appropriate decay paths C_- and C_+.

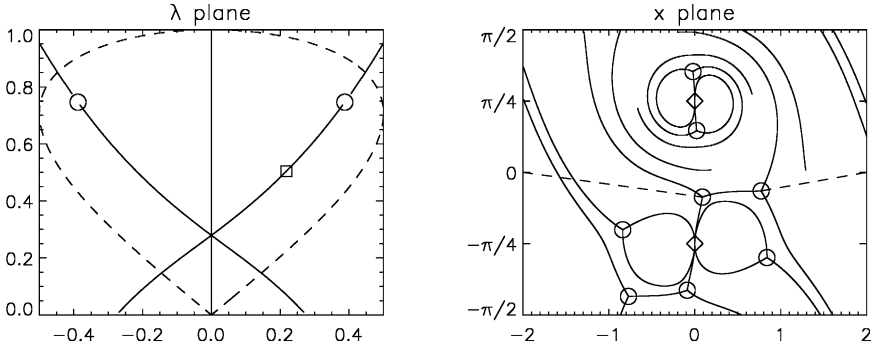

Fig. 11. The x-plane corresponding to a value of λ about halfway up a branch of the Y.

λ-plane. A plot of the critical orbits of (12) corresponding to a point roughly halfway along the graph between the triple intersection point and the branch point λ_D is shown in Fig. 11. As λ is moved very close to the branch point λ_D, trouble appears yet again on the horizon. As shown in Fig. 12, the double complex turning point that occurs at the branch point is clearly the coalescence of the turning points $x_2(\lambda)$ and $x_6(\lambda)$. The real path is correspondingly very short in this case. As λ is continued along the graph of $\Re(I_{26}(\lambda)) = 0$ through the branch point λ_D, the two turning points involved coalesce and separate in the orthogonal direction. Above the branch point, there is still a real path between the turning points as shown in Fig. 13. However, it is no longer possible to find appropriate decay paths C_- or C_+. This unfortunate situation continues along the whole portion of the graph of $\Re(I_{26}(\lambda)) = 0$ lying above the branch point.

We therefore come to the conclusion that all four prerequisites for WKB analysis on a contour (C_-, C_0, C_+) are satisfied for λ on that portion of the graph of $\Re(I_{26}(\lambda)) = 0$ lying between the triple intersection point and the branch point λ_D. The analogous statement applies to the graph of the relation $\Re(I_{16}(\lambda)) = 0$, which is the curve with negative slope in Fig. 3. This follows from the fact that for the potentials (23), reflection about the imaginary axis in the λ-plane corresponds to reflection about the imaginary axis in the x-plane. These two curve segments, taken together with the portion of the graph of $\Re(I_{12}(\lambda)) = 0$ for which WKB analysis can proceed, form a Y-shaped curve in the λ-plane. This curve coincides to the eye *exactly* with the accumulation locus of discrete eigenvalues observed by Bronski [2]. On this Y-shaped curve, the approximate eigenvalues are obtained as the solutions of the Bohr–Sommerfeld quantization rule (14).

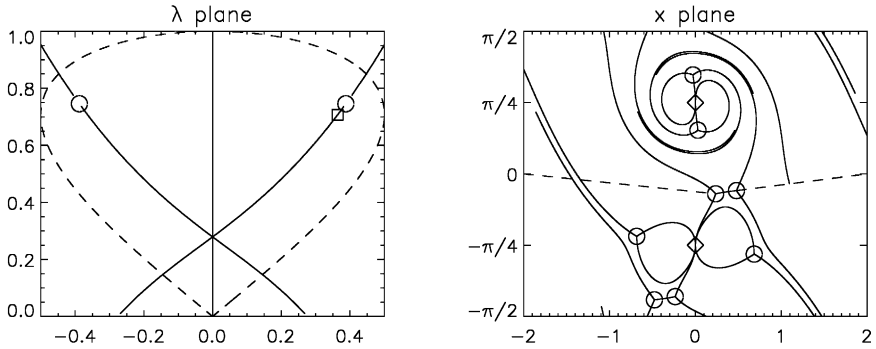

Fig. 12. The x-plane corresponding to a value of λ on a branch of the Y just below the branch point λ_D.

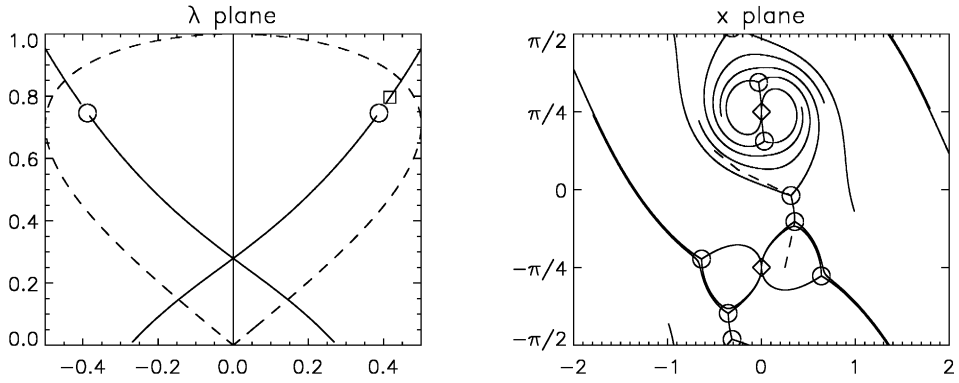

Fig. 13. The x-plane corresponding to a value of λ on a branch of the Y just above the branch point λ_D. Although there exists a real path between the complex turning points, there no longer exist appropriate decay paths C_+ and C_-.

Note that for the reader's convenience, we wanted to apply the method to potentials (23) that had been studied numerically in the literature [2]. In some respects, however, this particular choice is unnecessarily complicated. The transcendental nature of these particular potentials makes a direct exhaustive treatment impossible since there are an infinite number of possible pairs of complex turning points that might contribute a priori to the asymptotic spectrum. In view of simplicity, a better choice to illustrate the method might indeed have been rational potentials like $A(x) = S(x) = (x^2 + a^2)^{-1}$ for some $a \in \mathbb{R}$.

4. Application: ultrashort pulse generation in nonlinear optical fibers

One of the most important applications of the semiclassically scaled focusing nonlinear Schrödinger equation (2) is as a model for the all-optical generation of ultrashort pulse trains for subsequent modulation and transmission of high bit-rate signals in optical fibers. The idea is that electronic switching methods for creating trains of pulses are inherently frequency limited by the speed of the electronics, whereas the frequency of optical processes is potentially very large by comparison, and presents one avenue for the development of terabit per second transmission systems.

The semiclassical scaling of (2) occurs naturally in optical fibers, essentially because of the small ratio of the frequency of an electronic input signal and the frequency of an optical carrier. See [6] for a detailed discussion of this point. In optical fiber applications, the independent variable x is a retarded *time* coordinate for a disturbance $\psi(x, t)$ observed at a *distance* t along the fiber. Ignoring the initial condition for the moment, the soliton solution of (2) has duration (width in x) of $\hbar \ll 1$. It has an amplitude proportional to the imaginary part of the corresponding eigenvalue λ_k of (1) and a temporal shift per unit propagation distance (velocity $\mathrm{d}x/\mathrm{d}t$) proportional to the real part of λ_k.

Of course the initial condition $\psi(x, 0) = A(x)\exp(\mathrm{i}S(x)/\hbar)$ encodes a large number of solitons in the semiclassical limit. It has been pointed out [2,3] that the asymptotic spectral arcs essentially define *initial condition dependent nonlinear dispersion relations* for solitons in the semiclassical limit. That is, while for fixed $\hbar$ solitons can have any value of amplitude and velocity, these become highly correlated in the semiclassical limit, with the spectral arcs giving the asymptotic relation between one and the other.

For sufficiently chirped initial (temporally broad, electronically generated) pulses, we can suppose that the Y-shaped asymptotic spectrum is the rule. For such spectra, the evolution is quite complicated for propagation distances $t = \mathcal{O}(1)$. The nonlinear interference patterns of the solitons in this regime is the subject of current

investigations [7], and can be very regular [3,9] locally. But for longer propagation distances $t = \mathcal{O}(1/\hbar)$, while the field remains complicated in near the temporal center of the signal $x = 0$ due to the eigenvalues in the "neck" of the Y, isolated soliton pulses emerge far "upstream" and "downstream" for $x = \mathcal{O}(1/\hbar)$, corresponding to eigenvalues in the two branches of the Y. In the "window" of t and x both $\mathcal{O}(1/\hbar)$, one observes a rank-ordered train of ultrashort soliton pulses. Once these pulse trains are generated, they may be diverted and modulated to encode a data stream.

The utility of a tool that supplies the asymptotic spectral arcs given the analytic potentials $A(x)$ and $S(x)$ is clear for applications like the generation of pulse trains described here. Even more useful would be an associated "inverse" procedure, by means of which potentials $A(x)$ and $S(x)$ could be determined from prescribed asymptotic spectral arcs, say corresponding to the branches of the Y. For example, one could try to find functions $A(x)$ and $S(x)$ so that each branch of the Y had an isolated point with a vertical tangent. The pulses corresponding to the solitons with eigenvalues in the neighborhood of such a critical point would all be stationary in some frame of reference, and would be ideally adapted to minimizing the effects of the Gordon–Haus jitter instability.

Although the formula (13) for the asymptotic spectral arcs is complicated, certain features relevant to applications are easy to extract explicitly. In the limit of long propagation distances $t = \mathcal{O}(1/\hbar)$, the real part of the eigenvalue of the fastest soliton determines the asymptotics of the total size of the disturbance. In this connection, the formula (25) for the endpoints λ_{D} of the Y-shaped spectrum (more generally, λ values for which there exist double turning points in the complex x-plane), gives a simple way to characterize these gross features of the asymptotic disturbance. A general formula for this maximum field expansion rate, assuming only that the potentials $A(x)$ and $S(x)$ generate a Y-shaped asymptotic spectrum whose "branches" have finite nonzero slope, is given by the supremum of $\Re(\lambda_{\mathrm{D}})$ over all simultaneous solutions $(\lambda_{\mathrm{D}}, x)$ of the equations $V_0(x;\lambda_{\mathrm{D}}) = 0$ and $V_0'(x;\lambda_{\mathrm{D}}) = 0$.

5. Making some results rigorous

In this section, we speculate upon how one might prove an assertion like

Proposition 1. *Let K be a compact subset of an asymptotic spectral arc; suppose that K contains no points of intersection with other spectral arcs. There exists a constant $c_K > 0$ such that whenever $\lambda_0 \in K$ satisfies the Bohr–Sommerfeld quantization condition* (14) *and $\hbar$ is sufficiently small, there exists an eigenvalue λ of the Zakharov–Shabat problem* (1) *with $|\lambda - \lambda_0| \leq c_K\hbar^2$.*

If discrete eigenvalues can also be excluded from accumulating elsewhere in the complex plane, then with the $\mathcal{O}(\hbar)$ separation of the approximate WKB spectrum on the asymptotic spectral arcs, the convergence of the discrete spectral measure to the asymptotic spectral measure implied on each arc by the Bohr–Sommerfeld quantization rule (14) will follow as well. However, as noted above for some applications (e.g. semiclassical inverse-scattering theory) more precise control on each eigenvalue may be required.

In proving the proposition it seems advantageous to first work on the contour C associated with the spectral arc containing K and establish the validity of the WKB approximation for the reduced equation (8) in $L^2(C, \mathrm{d}s)$ where s is some real parameterization of C with $s \sim x$ for large x. Then, invoke analyticity of the solutions of (8) in the domain enclosed by the contour C and the real axis to obtain a solution in $L^2(\mathbb{R})$ of the same equation. Finally, perturbation theory will be necessary to put back the terms $\hbar^2 F_{\pm}(x;\lambda)$ and yield a solution of (5) in $L^2(\mathbb{R})$ and therefore an eigenfunction of (1).

The correct setting for the WKB approximation of bound state eigenfunctions on the contour C is the method of comparison equations [4]. Given that λ_0 lies on an asymptotic spectral arc, it is possible to find a global change of variables that transforms the reduced Schrödinger equation (8) into the parabolic cylinder equation with a small

bounded correction. One writes $y(x) = f(x)w(s(x))$ and chooses $f(x)^2 = 1/s'(x)$. If for some value of t,

$$t - s(x)^2 = -\frac{V_0(x;\lambda)}{s'(x)^2}, \tag{31}$$

then Eq. (8) becomes

$$\hbar^2 w''(s) + (t - s^2)w(s) = \hbar^2[\tfrac{1}{2}s'(x)^{-3}s'''(x) - \tfrac{3}{4}s'(x)^{-4}s''(x)^2]w(s). \tag{32}$$

The relation (31) will define an invertible change of variables mapping the contour C to the real s-axis if the turning points are made to coincide under the transformation. This will be the case if $t = t(\lambda_0)$, where

$$t(\lambda) = \frac{2}{\pi}\int_{x_-(\lambda)}^{x_+(\lambda)} \sqrt{-V_0(z;\lambda)}\,\mathrm{d}z, \tag{33}$$

where the path of integration is C_0 and the differential $\sqrt{-V_0(z;\lambda)}\,\mathrm{d}z$, real and nonzero by assumption, is taken to be positive. Note that this defines t as an analytic function of λ in the compact subset K of the asymptotic spectral arc under consideration; it may be analytically continued for λ in a fixed but small strip on either side of K. Under this change of variables, the error terms on the right-hand side of (32) can be reinterpreted as functions of s. These complex-valued coefficient functions are uniformly bounded in s.

We are assuming that not only does λ_0 lie on an asymptotic spectral arc so that the above transformation is possible, but also that λ_0 satisfies the quantization condition (14). This is equivalent to the statement that $t = t(\lambda_0)$ is an exact eigenvalue of the parabolic cylinder equation in $L^2(C,\ \mathrm{d}s)$. The unperturbed problem, (32) without the terms on the right-hand side, is thus completely understood; the spectrum is purely discrete ($t = 2\hbar(n + \frac{1}{2})$ for $n = 0, 1, 2, \ldots$) and nondegenerate. Analytic perturbation theory can be used to include the effect of the neglected terms on the right-hand side of (32). There is some complication because the change of variables $s(x)$ depends parametrically on λ and therefore on $t(\lambda)$, which is expected to change slightly under perturbation. Writing $t_0 = t(\lambda_0)$ and $\delta = t - t_0$, the perturbed problem can be expressed in terms of an operator $T_{\epsilon,\delta}$ of the form:

$$T_{\epsilon,\delta}w(s) = \hbar^2 w''(s) + (t_0 - s^2)w(s) - \{(\epsilon g(s;\delta) - \delta)w(s)\}, \tag{34}$$

where $\epsilon = \hbar^2$ and $\epsilon g(s;\delta)$ is the right-hand side of (32), including the dependence on $t(\lambda)$. We want to study the deformation of the simple eigenvalue t_0 using the Kato–Rellich theorem [8,10]. Most of the results of the Kato theory of analytic families of operators carry over to families depending holomorphically on *two* complex parameters. Consider $\hbar$ fixed. With respect to the complex parameters ϵ and δ, $T_{\epsilon,\delta}$ is an analytic family of type (A) [8]; this follows from the fact that the terms depending on the parameters are bounded on $L^2(C, \mathrm{d}s)$. Zero is an eigenvalue of $T_{0,0}$, and the Kato–Rellich theorem guarantees that there is for $|\epsilon|^2 + |\delta|^2$ sufficiently small a nondegenerate eigenvalue $\tau(\epsilon,\delta)$ of $T_{\epsilon,\delta}$ that is analytic in the two variables and satisfies $\tau(0,0) = 0$.

The eigenvalue $\tau(\epsilon,\delta)$ is constructed as a convergent Rayleigh–Schrödinger series. The radius of convergence of this series can be bounded below in terms of the size of the resolvent of the unperturbed operator on a small circle around the origin in the complex τ-plane; the circle must separate the spectrum [8,10] and thus must be $\mathcal{O}(\hbar)$ in diameter (this is a property of the spectrum of the unperturbed parabolic cylinder equation). The resolvent is obtained directly by variation of parameters using parabolic cylinder functions solving the unperturbed problem for t on the circle about t_0. Using this bound, the radius of convergence must be shown to be bounded below by a quantity sufficiently large to ensure the validity of the theory in the region of interest, when $\epsilon = \hbar^2$ for sufficiently small $\hbar$. An implicit function theorem argument can then be used to show that the condition $\tau(\epsilon,\delta) = 0$ defines δ as a function of ϵ, with $\delta(0) = 0$. Using estimates for $\tau(\epsilon,\delta)$ following from majorization of the series [8], it then must be shown that $\delta(\hbar^2) = \mathcal{O}(\hbar^2)$.

The Kato–Rellich theory, suitably adapted for analytic families depending on two complex parameters, therefore gives an exact eigenvalue $t = t_0 + \delta(\hbar^2)$ of the perturbed parabolic cylinder equation (32). Inverting (33) at this eigenvalue, one obtains a value $\tilde{\lambda}_0 = \lambda(t)$ for which the reduced Schrödinger equation (8) has an exact $L^2(C, \mathrm{d}s)$ solution. Since solutions of (8) are analytic where $V_0(x; \tilde{\lambda}_0)$ is, and since by assumption there are no singularities of the potential between the contour $C = (C_-, C_0, C_+)$ and the real x-axis, the bound solution for $\lambda = \tilde{\lambda}_0$ whose existence is guaranteed by the perturbation argument above can be analytically continued down to the real axis. If there had been singularities of $V_0(x; \tilde{\lambda}_0)$ in the way, it might be possible for the bound state solution to have intermediate branch points and therefore have no single-valued analytic continuation down to the real axis. Since we are assuming that C_- and C_+ coincide with the real x-axis for $|x|$ sufficiently large, this continuation is in $L^2(\mathbb{R})$. The perturbed value $\tilde{\lambda}_0 = \lambda(t)$ is therefore an exact eigenvalue of (8) posed on the domain of interest, the real x-axis. The distance between λ_0 and $\tilde{\lambda}_0$ is bounded as stated in the proposition if the estimates described above are satisfied. Note that under the process of analytic continuation down to the axis, the true eigenfunction of (8) may become exponentially large. This fact suggests the difficulty with any WKB method that involves only information about the potentials on the real x-axis.

Now it is possible to work on the real x-axis, where the functions $F_\pm(x; \lambda)$ are uniformly bounded as functions of x (they are unbounded on the contour C). One should now apply the Kato–Rellich theory once again to study the behavior of the eigenvalue $\tilde{\lambda}_0$ under the perturbation taking Eq. (8) to Eq. (5). Because the perturbation depends on the eigenvalue parameter λ, this case must be handled as before, using a $\mathbb{C}^2$ analytic family to study the deformation of a zero eigenvalue. This time, setting $\delta = \lambda - \tilde{\lambda}_0$ and $\epsilon = \hbar^2$, we study the operator family $\tilde{T}_{\epsilon,\delta}$ defined in $L^2(\mathbb{R})$ by

$$\tilde{T}_{\epsilon,\delta} y_\pm = \hbar^2 y_\pm'' - V_0(x; \tilde{\lambda}_0) y_\pm - \{(V_0(x; \tilde{\lambda}_0 + \delta) - V_0(x; \tilde{\lambda}_0) + \epsilon F_\pm(x; \tilde{\lambda}_0 + \delta)) y_\pm\}. \tag{35}$$

In principle, degeneracy could be introduced in the process of analytic continuation to the real x-axis because of interference of eigenvalues of (8) that are not captured by the WKB analysis on the arc containing λ_0 (for example, eigenvalues coming from a different pair of complex turning points). However, let us assume that the exact eigenvalue $\tilde{\lambda}_0$ of (8) is *not* degenerate. Then, the Kato–Rellich theory gives us an eigenvalue $\tilde{\tau}(\epsilon, \delta)$ of the operator $\tilde{T}_{\epsilon,\delta}$ that is analytic in ϵ and δ and satisfies $\tilde{\tau}(0, 0) = 0$. As before, it is necessary to estimate the radius of convergence of the Rayleigh–Schrödinger series for $\tilde{\tau}$ and use the implicit function theorem to obtain δ as a function of ϵ, valid out to $\epsilon = \hbar^2$ and bounded by a quantity of order $\hbar^2$. These estimates will be harder to obtain this time, because much less is known about the resolvent and separability of the spectrum of $\tilde{T}_{0,0}$ than before. In particular, there is some danger because in working on the real x-axis the known eigenfunctions may be exponentially large and therefore difficult to control; similar things could well be true about the unperturbed resolvent. Nonetheless, the agreement of the predictions of the method with numerical experiments suggests that such estimates can indeed be obtained.

6. Conclusion

In this paper, we have described how under the assumptions of real-analyticity of the potential functions $A(x)$ and $S(x)$, and sufficient decay of $A(x)$ and $S'(x)$ for large $|x|$, the WKB method can be complexified to determine certain *asymptotic spectral arcs* on which discrete eigenvalues of the nonselfadjoint Zakharov–Shabat eigenvalue problem are expected to accumulate in the limit of small $\hbar$. Once the arcs are found, a Bohr–Sommerfeld like quantization rule gives the distribution of eigenvalues on each arc. The method makes predictions that are verified by the numerical calculations of Bronski [2].

The method does not address whether there can be semiclassical eigenvalues in the neighborhood of a value of λ for which there is no contour (C_-, C_0, C_+) of the type described in the text. Although the procedure described

here is effective, it is not obvious that the asymptotic spectral arcs so obtained lie in the "shadow" of the turning point curve as required by the bound of Deift, Venakides, and Zhou.

Obviously, analyticity of the potential functions $A(x)$ and $S(x)$ is crucial for the analysis. The reliance of the method on analyticity suggests the extreme sensitivity of the results with respect to small changes of the potentials. Given analytic functions $A(x)$ and $S(x)$ may be modified by an analytic perturbation that is arbitrarily small in some reasonable norm on the real axis, and the perturbed potentials may have essentially different properties in the complex plane, and consequently the semiclassical spectra can be very unstable. This sort of phenomenon is well-known for nonselfadjoint Schrödinger operators [1,5]. The most obvious way to approximate the semiclassical spectrum for nonanalytic potentials $A(x)$ and $S(x)$ would be to analytically approximate the potentials on the real axis. In a scheme of, say, rational approximation, higher order approximants would involve an increasing number of complex turning points. The asymptotic spectrum of the approximants may become more and more complicated, consisting of more and more asymptotic spectral arcs, as the approximation improves. Through a limiting process, one can imagine that the asymptotic point spectrum for nonanalytic potentials may well be dense in two-dimensional regions of the complex plane. Indeed, this was foreseen by some and feared to be the case for all potentials prior to the publication of Bronski's numerical experiments.

Further instability may be expected in the asymptotic calculation of the proportionality constants, where there may be difficulty even for analytic potentials, as touched on in Section 2.3. Work in progress [7] on the semiclassical inverse-scattering problem for the focusing nonlinear Schrödinger equation suggests that small perturbations in the asymptotic distribution of the proportionality constants can lead to large contributions to the leading-order asymptotics (on the other hand, the semiclassical inverse theory seems to be fairly robust with respect to perturbations of the Bohr–Sommerfeld eigenvalue density). It is therefore very important for the analysis to be extended to include sufficiently accurate formulas for the γ_k.

References

[1] A. Aslanyan, E.B. Davies, Spectral instability for some Schrödinger operators, Numerische Mathematik 85 (2000) 525–552.
[2] J.C. Bronski, Semiclassical eigenvalue distribution of the Zakharov–Shabat eigenvalue problem, Physica D 97 (1996) 376–397.
[3] J.C. Bronski, J.N. Kutz, Numerical simulation of the semi-classical limit of the focusing nonlinear Schrödinger equation, Phys. Lett. A 254 (1999) 325–336.
[4] M.V. Berry, K.E. Mount, Semiclassical approximations in wave mechanics, Rep. Prog. Phys. 35 (1972) 315–397.
[5] E.B. Davies, Semi-classical states for non-self-adjoint Schrödinger operators, Comm. Math. Phys. 200 (1999) 35–41.
[6] M.G. Forest, K.T.-R. McLaughlin, Onset of oscillations in nonsoliton pulses in nonlinear dispersive fibers, J. Nonlinear Sci. 8 (1998) 43–62.
[7] S. Kamvissis, K.T.-R. McLaughlin, P.D. Miller, Semiclassical soliton ensembles for the focusing nonlinear Schrödinger equation, submitted to Ann. Math. Stud. (2000), http:/arXiv.org/abs/nlin.SI/0012034.
[8] T. Kato, Perturbation Theory for Linear Operators, Springer, Berlin, 1995.
[9] P.D. Miller, S. Kamvissis, On the semiclassical limit of the focusing nonlinear Schrödinger equation, Phys. Lett. A 247 (1998) 75–86.
[10] M. Reed, B. Simon, Methods of Modern Mathematical Physics IV: Analysis of Operators, Academic Press, Boston, 1978.
[11] V.E. Zakharov, A.B. Shabat, Exact theory of two-dimensional self-focusing and one-dimensional self-modulation of waves in nonlinear media, Sov. Phys. JETP 34 (1972) 62–69.